Long run experiments on high temperature molten carbonate fuel cells

G.H.J. Broers and M. Schenke

Central Technical Institute T.N.O., The Hague, Netherlands *)

1. INTRODUCTION

Research on high temperature fuel cells of the molten carbonate electrolyte type, by the Dutch organisation T.N.O., was taken up in 1950. The development of this work has been described in a series of publications [1] - [6]. Comments on the work can also be found in [7] and [8].

A significant step towards the realisation of the strictly necessary gastightness was made by the application of the so-called paste electrolyte [4], [5]. It is obtained by blending an inert powdered solid such as MgO with a given amount of binary or ternary alkali carbonate mixture (Li_2CO_3, Na_2CO_3, K_2CO_3).

Above the eutectic melting point of the carbonates (500°C for Li-Na; 396°C for Li-Na-K) a stiff and dense paste can be obtained when the inert solid to carbonates weight ratio remains above a certain critical value. This value depends on the particle size (and shape) of the solid constituent and the composition of the carbonate mixture. As a rough-and-ready rule, a 50 solid/50 liquid weight ratio will yield a rather stiff paste when the particle size of the solid (MgO) is below 1 micron; but closer readjustments have to be made in accordance with the basic materials used. A too high liquid content will cause plastic flow, a too low one causes an unnecessarily high electrolyte resistance. Under optimal conditions, the specific resistance of a typical MgO/ternary carbonate paste is about two times as large as the corresponding pure liquid resistance (paste resistance $\sim 1.5\ \Omega$ cm at 700°C).

The experiments to be discussed here were all conducted on a laboratory scale. It was felt that technological development work was justified only if, in addition to leaktightness, the following demands could be satisfied:

1) a specific power output of at least 50 mW/cm^2 at 0.5 volt or better,
2) fuel and oxidant utilisation of at least 80%, at current densities of the order of 100 mA/cm^2,
3) a cell life of at least several months at the just mentioned power output, with the aim of reaching a life of the order of three years [6], [9] in future developments.

2. CELL CONSTRUCTION, ELECTRODES AND FUELS

For purposes of fundamental research, a high temperature cell should meet the following demands: 1. perfect gastightness; 2. absence of any parasitic current paths, such as caused by metallic gaskets in contact with the electrolyte; 3. reliable contacts between the electrodes and the electrolyte; 4. presence of a suitable reference electrode, connected to the system by some form of electrolytic bridge; 5. no galvanic contacts with the surrounding heating furnace; 6. appriopriate means to know the degree of galvanic turnover, that is the ratio of the Faradaic current to the fuel and oxidant feed rate.

---

*) Correspondence on this subject to the laboratory address: 198, Hoogte Kadijk, Amsterdam-C, Netherlands.

2.1. Cells

The mentioned demands are satisfactorily met by the constructions shown in Fig. 1 and Fig. 2. In Fig. 1 the paste disc is pressed firmly against the inner wall of a high-purity Al_2O_3 tube at about 500°C. There is virtually no reaction between the alumina material and the carbonate melt when the former has been pretreated with a small quantity of molten carbonate for a few days. The working electrodes are pressed against the electrolyte by means of two additional Al_2O_3 tubes with a number of openings at the side of the electrodes, providing gas passages from inside to outside or conversely.

The pressing force on these tubes can be carefully controlled by means of springs with screw adjustments at their cold ends.

The reference electrode is a Pt or Au wire, dipping into a Al_2O_3 capillary filled with electrolyte paste. This "paste bridge" serves as a Haber-Luggin type connection to the disc surface. The phase boundary of the reference wire thereby is effectively screened from the electrolyte disc proper, and no ill-defined stray currents can pass through the reference wire, such as is most likely the case with so-called "idle electrodes". (The latter have their phase boundary situated direct in the current path between the working electrodes.) The reference is flushed with the same gas as the working electrode.

Two lead wires may be connected to each of the working electrodes, one serving as current lead and the other as potential lead. Resistance changes of each individual electrode can thus be measured too.

Fig. 2 depicts a simplified version of the cell of Fig. 1, being easier to assemble (as is evident from the figure). In this version, the reference electrode is a Pt wire wrapped around the outside of one of the gas sealing Al_2O_3 tubes. Use is made of the (in itself tedious) "creeping" effect of the carbonate melt along the wall of the tube. The "creeping film" stabilises within one or two days of cell operation (it comes to a stop at the colder parts of the tube) and forms a very effective electrolytic bridge between the wire and the ring-shaped periphery of the paste disc.

Whereas in Fig. 1 the reference potential is equal within $\pm$ 5 mV to the corresponding working electrode potential at open circuit, the reference potential in Fig. 2 depends on the gas atmosphere in the heating furnace. Addition of a small CO_2 flush to the air inside the furnace yields very stable potentials.

Great care must be taken to avoid direct contact between any hot parts of the cell and the (a.c. heated) furnace. The just mentioned "creeping" may otherwise lead to severe hum pick-up and electric leakage to either the a.c. mains or the ground.

2.2. Electrodes

The porous fuel electrodes discussed in this paper were all nickel specimens of various origin. Screens, sieve plates, sintered carbonyl nickel, nickel plates for secondary batteries* and "fiber nickel"** plates were used, as well as presintered nickel powder obtained by

---

* E.g. "Clevite" porous Ni; Clevite Corporation, Cleveland, Ohio, U.S.A.

** Huyck Corporation; Milford, Connecticut, U.S.A.

reduction of NiO with H_2. The commercially available types have no special advantages over Ni powder electrodes and are, at least at the present-day prices, by far too expensive to be used for anything else but research purposes.

The porous air electrodes were either of silver or copper oxide.

Silver electrodes were used in the form of wire screens and/or very thin layers of Ag powder (0.1 mm or less), adhered direct to the electrolyte surface.

The use of CuO as air electrode was reported by Justi and co-workers [7], [10], in connection with work on solid carbonate electrolyte fuel cells. In our case, commercially available CuO powder was mixed with some 10% of Cu powder. Small discs of about 1 mm thickness were pressed and subsequently sintered at 800°C in an air atmosphere. In the first few experiments, the discs were connected to all-copper current leads, in order to make sure that the electrochemical activity could be attributed solely to the CuO - Cu_2O system. In later tests, current leads of stainless steel or Pt wires were connected to the CuO material, thus avoiding gradual oxidation of the leads in long run experiments.

Whereas in low temperature cells the initially chosen porosity, pore size distribution and electro-catalytic activity of the electrodes is of crucial importance, a quite different situation exists in high temperature cells. Sintering effects, anodic dissolution and cathodic precipitation, and both surface- and bulk oxide formation under varying polarization strongly tend to alter the initial electrode structure. Figs. 3a and 3b show nickel anode specimens before and after use respectively. Initially, the commercially available material* had a porosity of 70% and a thickness of 1.0 mm. Fig. 3a is a microphoto of this material. Fig. 3b similarly shows the same material after 625 hours of continuous operation at 700°C and (nominally) 100 mA/cm^2, on an equilibrium mixture of H_2, CO, H_2O and CO_2. (iR-free polarization about +110 mV relative to open circuit.)

The thickness had shrunk to 0.6 mm (40% decrease) and a lateral shrinkage of about 15% was observed.

Evidently it is of no use to preselect electrode structures for high temperature cells on any basis different from long term operation experience. One might state that the high temperature cell tends to seek its own operating level, and not the one preferred by the investigator on the basis of initial electrode structures.

Also, conclusions about cell performances over periods of a few days have little meaning. Both overoptimistic and overpessimistic impressions may then result. An example of the latter will be shown in Sec. 3, Fig. 5.

2.3. Fuels

In most of the experiments a "standard fuel" of 1 mole of H_2 + 1 mole of CO_2 was used. The "standard oxidant" was 2.5 (vol.) air + 1 (vol.) CO_2. The feed rate was usually chosen in such a way that at 100 mA/cm^2, 10 per cent of the fuel and the oxidants were consumed. The cells were operated at atmospheric pressure.

*) Sintered nickel, type J.E.G.V.; Mond Nickel Company, London, England.

The overall cathodic and anodic reactions can be written as

cathode: $2\ N_2 + \frac{1}{2}\ O_2 + CO_2 + 2\ \lambda\ e^- \rightarrow$

$$\rightarrow 2\ N_2 + \tfrac{1}{2}\ (1-\lambda)\ O_2 + (1-\lambda)\ CO_2 + \lambda\ CO_3^{=} \qquad (1c)$$

anode : $H_2 + CO_2 + \lambda\ CO_3^{=} \rightarrow$

$$\rightarrow (1-\lambda)\ H_2 + (1+\lambda)\ CO_2 + \lambda\ H_2O + 2\ \lambda\ e^- \rightarrow \text{equilibrium fuel} \qquad (1a)$$

λ is the conversion degree of the reactants; the composition of atmospheric air is taken for convenience as $2\ N_2 + \frac{1}{2}\ O_2$.

Although the $1\ H_2 + 1\ CO_2$ fuel is not in thermodynamic equilibrium at the inlet of the cell, it turns out that at the Ni anode the equilibrium is indeed established. In the first place, the less convenient to handle fuel $1\ CO + 1\ H_2O$ yields the same open circuit potential as the forme one. Secondly, this open circuit potential E is virtually equal to the value calculated on the basis of the equilibrium fuel composition and the Nernst law (decadic logarithm):

$$E\ (\text{volts}) = E_o(H_2) + 0.992 \cdot 10^{-4}\ T \log \left[\frac{p_a(H_2)\ p_c^{\frac{1}{2}}\ (O_2)\ p_c(CO_2)}{p_a(H_2O)\ p_a(CO_2)} \right] \qquad (2)$$

where p_a and p_c refer to anodic and cathodic partial pressures respectively.

For $\lambda = 0$ in eqs. (1c) and (1a), the calculated E values are 968 mV at 1000°K and 980 mV at 700°C [6]. The observed values at 700°C are between 970 and 985 mV, apart from initial deviations due to "non-aged" Ni electrodes. It will be shown in Sec. 4 that the standard fuel can be considered as being oxidised already for 32% with regard to an "optimal fuel", just not depositing carbon at 1000°K.

In some of the experiments, $CH_4 + CO_2$ mixtures were used. Usually, equilibrium in that case is not established at the Ni electrodes, but insertion of a small amount of commercial Ni on MgO reform catalyst, in the anode space, is sufficient to yield equilibrium.

3. OPERATING CHARACTERISTICS AND POLARIZATION EFFECTS

The cells under discussion were all kept under a continuous current drain of 100 mA/cm^2 (whenever possible), unless current vs. voltage curves were measured. The latter measurements were carried out over time intervals of at least a full hour, so that a steady state was always achieved.

Individual electrode polarizations could be measured with the aid of the reference electrode, using a mercury-wetted relay for fast ($\approx$ 2 μsec) current interruption and a Tektronix type 535A oscilloscope to measure iR drops and potential/time transients. The method is essentially similar to the one described by Trachtenberg [11] and makes use of the "sweep delay" provision of the C.R.O. time base, to observe the magnitude of the iR break conveniently and quite sharply.

The principle of the measurement may be clear from Fig. 4a, where a typical course of the electrode potentials has been plotted on a linear time scale, for two different current densities before interruption.

Fig. 4b shows the corresponding cathodic and anodic transienst plotted on a $t^{\frac{1}{4}}$ scale. The meaning of the partial linearity of these plots will be discussed hereafter.

Fig. 5 shows the steady state (iR free) potentials and the iR drop, as functions of the current density, of a cell at 740°C with a "fiber nickel" anode and a silver powder cathode. The x x points refer to the third day of operation. It is seen that the Ni anode potential positivates "dangerously" at about 80 mA/cm^2, whereas the Ag cathode potential varies linearly with the current. Also, the open circuit voltage of the cell, 1035 mV, is too high, 960 mV being the true equilibrium value [6].

The open circle points, taken after 18 days of operation, reveal a rather striking improvement of the anode, now polarising linearly with the current up to 160 mA/cm^2, where the polarization is +105 mV*. The Ag cathode also shows some improvement, the polarization being -76 mV at 160 mA/cm^2. The open circuit voltage now shows the proper value, 960 mV, indicating that the fuel gas attains true equilibrium at the "aged" electrode. The iR drop obviously has not changed during the operation period of 18 days.

The figure clearly shows the relative importance of electrode polarizations and iR drop; at 160 mA/cm^2:

iR drop = 340 mV > anode polarization = 105 mV > cathode polarization = 76 mV.

Fig. 6a shows similar results for a cell with a CuO cathode on the 27th day of operation at 720°C. At 200 mA/cm^2:

iR = 325 mV > an.pol. = 102 mV > cath.pol. = 70 mV.

Both anodic and cathodic polarizations are linear with the current density.

Fig. 6b shows a number of terminal voltage vs. current density characteristics for the same cell, taken at different times and for different fuel feeds. The line 27 in Fig. 6b corresponds with Fig. 6a. Line 13, on CH_4 + CO_2, in the absence of a reform catalyst, reveals that in this case no equilibrium is established at the Ni electrode, otherwise a much higher open circuit potential would have been observed (about 1100 mV). Nevertheless, upon current drain a reasonable performance can be obtained. (Addition of a few tenths of a gram of reform catalyst in the anode space yields the calculated open circuit value and correspondingly improved results.)

The line 28, on pure hydrogen, was taken on the last day before deliberate termination of the test period, with the main purpose to test the leak-tightness. The very high open circuit potential (1470 mV) shows the absence of any significant leakage after 4 weeks of operation. Also the capability of the CuO cathode to deliver current densities of 250 mA/cm^2 at about 90 mV polarization (on air + CO_2) could be demonstrated by this test.

The use of thinner electrolyte discs (9 mm in the case of Fig. 5 and 6.5 mm at Fig. 6) yields improved performances. The results shown in Fig. 4a, for instance, were obtained with a paste disc of 5 mm thickness. The terminal voltage in this case is 695 mV at 129 mA/cm^2 and still 540 mV at 212 mA/cm^2, with an iR drop of 282 mV in the latter case.

The given examples show that the purely resistive iR drop is always the predominant term in the total voltage drop of a current delivering cell. Nevertheless, the electrode polarization is by no means negligible, and therefore it is interesting to know whether it is mainly due to mass transport phenomena or to activation controlled processes (slow electron transfer, slow adsorption or desorption). A rather extensive study on this question has been

*) Polarization with respect to open circuit anode potential.

made by the present authors, but its details fall beyond the scope of this article and will be presented elsewhere [12].

Here it may be sufficient to note that d.c., a.c. and pulse methods, applied to both "flat" model electrodes (in the form of smooth wires or strips) and porous Ni and Ag electrodes, all point to mass transport controlled polarization (at least, above 600°C). Closer study reveals that the limiting factor is the presence of fluid electrolyte films on the surface of the electrodes, through which the reactant and product gases have to diffuse. At the Ni anode, the "off-diffusion" of the products CO_2 and/or H_2O through the film is rate determining, unless the H_2 partial pressure becomes very low (Sec. 4). At the Ag cathode the diffusion of either O_2 or CO_2 (depending on the relative partial pressures), is determining.

Evidence for the diffusion controlled character of the reactions at the porous electrodes is shown in Fig. 4b and Fig. 7. Though the porosity of the electrodes is ill defined, their properties may be approximated mathematically by the model of an "infinitely long" homogeneous transmission line [16].

Provided that the polarization tension at any spot on the phase boundary of the porous electrode is small enough as to yield an essentially linear relation between the instantaneous local tension and the corresponding current density, a mathematical analysis of the transmission line model yields the following results [12]:

1) Steady state. If the specific phase boundary resistance* of a planar electrode is R_b ($\Omega\,cm^2$), the corresponding effective resistance R_p of a porous electrode is proportional to $\sqrt{\rho\,\delta\,R_b}$, where ρ is the specific resistance of the electrolyte film and δ its thickness.

2) Alternating current impedance. Similar to 1), if the phase boundary impedance of a planar electrode is $Z_b = A - jB$, where A is the real and B the imaginary component of Z_b and $j = \sqrt{-1}$, then the corresponding impedance Z_p of a porous electrode is proportional to $\sqrt{\rho\,\delta\,Z_b}$.

3) Galvanostatic transient response. It is well known that for a diffusion controlled process at a planar electrode, the overtension v, resulting from a short constant current pulse Δi, changes proportional to the square root of time:

$$v = \text{const.}\ \Delta i\ \sqrt{t}.$$

For the transmission line model of the porous electrode the corresponding relation can now be written as:

$$v = \text{constant}\ \Delta i\ \sqrt{\rho\,\delta}\ t^{\frac{1}{4}}$$

Now Fig. 4b depicts the course of anodic (porous Ni) and cathodic (porous Ag) polarization tensions after current interruption**, as functions of $t^{\frac{1}{4}}$. It is seen that the curves for both 129 mA/cm^2 (geometrical current density) and 212 mA/cm^2 show linear portions, as predicted by the latter formula. Moreover, the slopes of these linear portions are proportional with the current density, both for the anodic and cathodic curves. The anodic and

---

* The phase boundary resistance is defined as the ratio of polarization tension to current density. The concept is valid for small polarizations only ($< RT/F$).

** In order to observe the polarization change accurately, oscilloscopic traces were photographed over time intervals of 10^{-4}, 10^{-3}, 10^{-2}, 10^{-1} and 1 second.

cathodic slopes for the same current density, however, are different. It is seen that the anodic response is considerably more sluggish than the cathodic one.

The deviating initial part of the anodic curves (the first 5 milliseconds) is probably due to the interference of double layer capacity effects.

Fig. 7 is a so-called Argand diagram of the impedance $Z_p = A_p - j\,B_p$ of a nickel brush electrode. In the diagram, the real part A of the observed electrode impedance has been plotted against the imaginary part B, for different a.c. frequencies between 10 c.p.s. and 50 kc.

For a purely diffusion controlled process at a planar electrode, the phase boundary impedance Z_b is the so-called Warburg impedance: $Z_b = W_o\,\omega^{-\frac{1}{2}} \exp - j\,\pi/4$; where W_o is a constant, ω the angular a.c. frequency and $\pi/4 = 45^o$ the phase angle (arc tan B/A). According to 2), the corresponding impedance Z_p of the porous electrode should now be proportional to $\sqrt{Z_b} = W_o^{\frac{1}{2}}\,\omega^{-\frac{1}{4}} \exp - j\,\pi/8$. In the Argand diagram of the impedance vector end points, the latter expression is represented by a straight line with a slope $\pi/8 = 22\frac{1}{2}^o$, and $|Z_p|\,\omega^{\frac{1}{4}}$ = constant. It is seen that the observed impedances satisfy these demands only approximately, with the greatest deviation at high frequencies. When, however, a correction is made for the influence of the double layer capacity (by standard vectorial subtraction methods) the cross-points are obtained, which satisfy the theoretical prediction very well. Similar results have been obtained for porous anodes with less ideal geometry than the brush form of the presented example.

The occurrence of the square root form $\sqrt{\rho\delta}$ in the various expressions for the polarization implies that the measured polarization always includes a purely resistive contribution from the electrolyte film. Moreover, since the true phase boundary resistance R_b only appears as $\sqrt{R_b}$ in the expression for the steady state polarization of a porous electrode, the latter will be relatively insensitive to small variations of R_b, such as can be expected for slightly non-linear voltage-current relations. And finally, because RT/F at 1000°K has the large value of 87 mV, it is not very surprising after all that the observed steady state polarizations (Figs. 5 and 6) are essentially linear with the current density.

4. FUEL AND OXIDANT UTILISATION

4.1. Oxidation of the fuel

In the experiments of Sec. 3, the fuel and oxidant utilisation was of the order of 10%, at about 100 mA/cm^2, relative to the feed. With regard to the fuel, the general course of its oxidation by $CO_3^=$ ions can be visualised conveniently in the triangular C-H-O diagram of Fig. 8.

The "standard fuel" 1 H_2 + 1 CO_2 is represented by P. Its oxidation (cf. reaction (1a), Sec. 2.3) proceeds along the straight line P - CO_3, and would be completed at point P_e. Considering P as the initial fuel, its conversion degree λ at P is zero, and $\lambda = 1$ at P_e on the line H_2O - CO_2. The "optimal fuel", however, which can be oxidised along the same path, is represented by P_o on the carbon deposition boundary (C.D.B.) curve [6], [13]. At 1000°K and 1 atm total pressure the composition of P_o is 0.17 C + 0.63 H + 0.20 O. Is is easy to show that, with respect to oxidation by $CO_3^=$ ions, the standard fuel P is already oxidised for 32% when P_o is taken as the initial fuel. If λ_o represents the conversion degree of P_o, then $\lambda_o = 0.32 + 0.68\,\lambda$ (λ = conversion degree of P).

It is possible to calculate the theoretical (Nernst) EMF for any value of λ or λ_o, by means of equation (2), Sec. 2.3 when the equilibrium compositions of the C-H-O gas phase on the line $P_o - P_e$ are known. The author (Broers) has found a simple method [14] to calculate curves of constant CH_4 partial pressure (Fig. 8) and curves of constant EMF (Fig. 9) in the triangular diagram, so that the theoretical EMF values for different points on the line $P_o - P_e$ can be read directly from it.

The CH_4 "isobars" of Fig. 8 show that at 1000°K, in the range of interest, $p(CH_4)$ is rather low, so that in good approximation only the equilibrium:

$$H_2 + CO_2 \leftrightharpoons H_2O + CO$$

needsto be considered. This makes calculations of the equilibrium compositions along the path $P_o - P_e$ fairly simple.

A still more convenient method involves the use of the diagram of Fig. 9. The curves in this figure permit a direct reading of the "excess EMF", ΔE (in millivolts), which has to be added to $E_o(H_2)$, cf. equation (2), to obtain the E value with regard to anodic gases. The cathodic contribution in (2) can of course be calculated straight forwardly.

The course of the <u>theoretical</u> EMF along the path $P - P_e$, i.e. $\lambda = 0$ to $\lambda = 1$, is shown in Fig. 11, upper curve. The cathodic partial pressures $p_c(O_2)$ and $p_c(CO_2)$ are kept constant (0.14 atm and 0.28 atm respectively), in agreement with the experimental set-up to be described.

Now the course of the <u>practical</u> cell terminal voltage as a function of λ was determined as follows. Suppose we have a battery of n cells, of equal surface area, connected in series. The fuel is passed through this battery in series flow. Then each cell converts a fraction $\Delta\lambda$ of the fuel, at equal current density. When the current is i, and the feed rate of the combustible part of the fuel mixture is equivalent to n i, $\Delta\lambda = 1/n$. The overall conversion degree at the <u>entrance of cell k</u> will be $\lambda = (k - 1)/n$, and <u>at its exit</u> $\lambda = k/n$. Thus, in principle the conversion would be complete at the exit of cell n. In practice this cannot be realised, since progressive fuel depletion and product accumulation tend to increase the (mass transfer controlled) polarization, so that in some given cell of the battery the actual current density becomes the limiting one.

Since no practical battery was available, relevant experiments were carried out with a single cell at 720°C, by means of a simulator technique represented in Fig. 10. When the standard fuel has been oxidised to a degree λ, reaction (1a), Sec. 2.3 has occurred.

In order to realise this reaction, the necessary amount of "$CO_3^=$ ions" was supplied to the fuel in the form of gaseous O_2 and CO_2 (in the proper ratio), so that the latter gases reacted directly in the hot part* of the anode tube with the incoming fuel, before reaching the electrode.

The supposed number of cells n was chosen as 10. At a cell current i the H_2 feed was evolved electrolytically at a current 10 i, and the additional equal CO_2 feed (O_2 free) by accurate flow meter adjustment. O_2 simultaneously was evolved and supplied electrolytically at a current 10 λi, and mixed with an equivalent flow of 10 λ i CO_2 (the double amount of CO_2 against O_2 when expressed in moles/second). Thus the conversion

---

* Compare Fig. 2, $O_2 + CO_2$ entering through auxiliary inlet.

of the fuel could be adjusted quite accurately, by ammeter readings.* The oxidant flow rate was held constant, at a large excess, in order to keep the cathode potential constant.

The results, at current densities of 62 mA/cm^2 and 125 mA/cm^2 are shown in Fig. 11. Since $\Delta\lambda = 0.1$ and e.g., at the entrance of cell no. 4, $\lambda = 0.3$, the voltage reading of cell 4 has been plotted at $\lambda = 0.35$. The actual voltages observed (full curves) have also been corrected for iR drop, yielding the dashed curves. It is seen that:

1. At 125 mA/cm^2 about 70% of the standard fuel (P in Fig. 8) can be utilised, or about 80% of the corresponding optimal fuel (P_o in Fig. 8; λ_o axis in Fig. 11). The partial pressure of the remaining fuel at $\lambda = 0.7$ is 0.11 atm.
2. At 62 mA/cm^2, 90% of the standard fuel, or 93% of the optimal fuel can be utilised. The partial pressure of the remaining fuel at $\lambda = 0.9$ is 0.034 atm.
3. The difference between the theoretical E curve and the dashed curves, that is the polarization, appears to decrease with increasing fuel conversion, till close to the point where the current density becomes the limiting one.

This rather surprising phenomenon may be explained by the already known fact that not the fuel, but the products CO_2 and H_2O are rate controlling (Sec. 3), and that the overall rate of gas flow increases with increasing conversion (equation 1a). Probably the effect of the increasing CO_2 and H_2O partial pressures is counteracted so much by the increasing flow rate, that the overall effect is in favour of a polarization decrease. But finally the mass transport of the H_2 + CO fuel, now at rather low partial pressure, takes over the role of the reaction products, and total depletion at the electrode surface starts very soon thereafter.

These observations clearly show that the attainable fuel utilisation is a pronounced function of the current density. In order to use the greatest possible fraction of the fuel feed, the current density in the "last cells" of the battery has to be decreased by increasing their surface area. Practically, this becomes a matter of optimising the increasing investment costs against the decreasing fuel costs. In this sense, the possibility of 90% fuel utilisation at (at least) about 60 mA/cm^2 seems a rather encouraging result.

4.2. Utilisation of O_2 and CO_2**

The conversion at the cathode is given by equation (1c), Sec. 2.3.

The experimental measurement of the terminal voltage as a function of λ in an imaginary 10 cell series battery was carried out as follows:

1. Excess fuel (1 H_2 + 1 CO_2) was used at the anode (about 10% conversion).
2. At cell current i, an electrolytically generated O_2 feed, 10 $(1-\lambda)$ i, was led into the cathode space of the cell, together with:
3. A CO_2 feed (O_2 free) of 10 $(1-\lambda)$ i, that is twice the O_2 flow rate in volume/sec.
4. A N_2 feed (O_2 free) held constant at 4 times the oxygen volume flow rate for $\lambda = 0$.

---

* Also to λ values not corresponding with integral cell numbers.

** The experiments described here and in Sec. 4.1 were carried out with one cell, with a Ag powder cathode and a "fiber nickel" anode. The measurements lasted 17 days in all.

The theoretical voltage as a function of λ was computed easily from the Nernst Law (equation (2), Sec. 2.3), using (1c) to calculate $p_c(O_2)$ and $p_c(CO_2)$. The results, at 720°C, are shown in Fig. 12, for current densities of 125 mA/cm^2 and 62 mA/cm^2. The dashed curves represent the iR free voltages. It is seen that:

1. At 125 mA/cm^2, about 85% of the "oxidant" $\frac{1}{2}\,O_2 + CO_2$ can be utilised. At this conversion, the remaining partial pressures are: $p(O_2) = 0.034$ atm; $p(CO_2) = 0.067$ atm.
2. Similarly at 62 mA/cm^2, about 95% utilisation is possible; $p(O_2) = 0.012$ atm; $p(CO_2) = 0.024$ atm.
3. By maintaining a slight excess of O_2 at 125 mA/cm^2, corresponding with $\lambda(O_2) = 0.80$, and studying the effect of $\lambda(CO_2) \geq 0.80$ solely, the dotted curve was found. Thus with regard to CO_2 conversion, about 90% can be utilised at 125 mA/cm^2.
4. Conversely, by keeping $\lambda(CO_2)$ at 0.80 and increasing $\lambda(O_2)$ beyond this value, about 93% O_2 utilisation could be reached. It seems therefore that in fact CO_2 is limiting when the stoichiometrical O_2/CO_2 ratio is used, but the match is rather close and may fall within the accuracy of the CO_2 flow meter calibration.
5. In contrast with Fig. 11, increasing conversion now brings about slightly increasing polarization, up till $\lambda \approx 0.75$. Since the overall flow rate in this cathodic case decreases with increasing λ, this is the result to be expected. Nevertheless, the polarization increase is enjoyably small.

From a purely theoretical standpoint, the maximum possible O_2 depletion from the air feed is not very important, though a great excess of air is definitely unwanted in connection with the heat balance of a battery system.

A quite different situation pertains to CO_2 depletion. Consider the (assumedly) complete combustion of a hydrocarbon C_nH_{2n+2}. The overall anode reaction is:

$$C_nH_{2n+2} + (3n+1)\,CO_3^{=} \rightarrow (4n+1)\,CO_2 + (n+1)\,H_2O + (6n+2)\,e^- \qquad (3)$$

Now the oxidation products are to be recycled to the cathode, and mixed with air in such an amount that at least $(3n+1)\,CO_3^{=}$ can be formed and also utilised. Since $(4n+1)\,CO_2$ is available, its conversion degree should be at least:

$$\lambda(CO_2)_{cath.} \geq (3n+1)/(4n+1)$$

Thus the cathodic conversion degree of CO_2 should be better than 80% for methane fuel, and still better than 75% for higher hydrocarbons ($n \gg 1$). The experiments depicted in Fig. 12 show that conversion degrees of this magnitude can indeed be attained at current densities up to 125 mA/cm^2.

To the knowledge of the authors, experiments of the kind discussed here have not been reported earlier. Only Chambers and Tantram [15] reported data on H_2 conversion percentages, but did neither specify the current density nor the actual terminal voltages observed.

5. LONG RUN EXPERIMENTS AT CONSTANT CURRENT DENSITY (100 mA/cm^2)

In earlier work [5], [6], it was not possible to draw current densities of the order 100 mA/cm^2 for more than about 1 week. Improvement of the electrolyte paste properties eliminated the instability effects at current densities > 25 mA/cm^2 virtually completely, so that a long run test at 100 mA/cm^2 could be carried out on a pair of small "twin cells" of 1 cm^2 surface area each.

Standard fuel and oxidant were used at 700°C, with 10% conversion relative to their feed rates. Both cells had "reinforced" Clevite porous nickel anodes (initially 70% porosity), which were used without any pretreatment. The cathodes were silver screens (0.5 mm wires with equally large spacings); cells constructed as shown in Fig. 1.

Fig. 13, upper section, shows the results over a 4600 hours period (after which the measurements were terminated deliberately), in terms of 1. terminal voltages, 2. iR free voltages, 3. open circuit voltages. The latter were observed only occasionally; see points indicated.

It is seen that:

1. The performances run rather similarly, the terminal voltages decreasing slowly from about 750 mV initially down to 470 mV at 4600 hours.
2. The iR free voltages become practically constant after 2-2½ months, so that the electrode polarizations also become constant after that period. The cathodic polarizations (not shown separately from the anodic ones) stabilise to about 50 mV, the anodic ones to about 150 mV.
3. Initially there is an increase in polarization, which has to be ascribed to alterations of the porous Ni anodes. (Sintering effects, compare Figs. 3a-3b, Sec. 2.2). With respect to these alterations, "ageing" of the electrodes by a heat pretreatment at 800°C, in reducing atmosphere, is rather favourable.
4. The open circuit voltages (initially too high) attain the calculated value 980 mV within about 2 weeks, up till the end of the test. This indicates that the cells were still gastight after 6 months.

Analysis of the electrolyte pellets revealed that about 50 mole % of the initial carbonate content was lost after the 6 months period. In Fig. 13, lower section, the conductivity of cell 3 (cell 2 gives similar results) has been plotted as a function of the operating time. It is seen that, roughly speaking, the decrease of the conductivity is proportional with time, and that from 500 to 4500 hours a 50% decrease has occurred. This suggests that the only cause of the performance decrease, after the "stabilising period" of the anode, is due to slow vaporisation of the carbonate melt.

In principle, carbonate losses may occur by "creeping" as well as by vaporisation. In the conditions of the experiment, however, creeping of the Li-Na-K carbonate melt comes to a stop at the cold parts of the alumina tubes, within one or two days. Moreover, it is very unlikely that losses through creepage would alter the ratio of Li to Na to K.

The chemical analysis of the used electrolyte pellets, however, proved that the mentioned ratio had changed considerably. Initially the alkali atom fractions were : 0.37 Li, 0.39 Na, 0.24 K,
whereas after 6 months they were : 0.47 Li, 0.36 Na, 0.17 K.

Thus the rate of K evaporation is the largest, that of Li the smallest one. Though the relative order of alkali carbonate stability is just the reverse with regard to CO_2 vapour pressure [1], it should be kept in mind that in the present experiments a relatively large CO_2 partial pressure was maintained all the time on both sides of the electrolyte pellet.
(A blank experiment with a liquid Li-Na-K carbonate mixture under CO_2 of 1 atm at 700°C, using a "cold finger" to condense the vapours, yielded qualitatively similar results. It took several weeks to collect a small quantity of condensed vapour.)

On the basis of the total amount of fuel and oxidant gases passed over the electrolyte pellets in the test period, it can be calculated that 1 mole of CO_3 was lost per (about) 10^5 moles of fuel, air and CO_2. Thus the vaporisation rate is quite small.

This in turn would mean that a (more or less) continuous supply of fresh melt in very small quantities would result in a practically constant performance over a period of several times the one observed here, that is in the order of at least a few years.

In conclusion, it may be stated that with regard to power output, attainable gas utilisation and life of the essential cell components, the prospects of the high temperature fused carbonate cell are far more favourable than thought hitherto.

Only work on a larger scale can show whether the construction of batteries is technically, and if so, also economically feasible. The authors fully appreciate that this still a long way to go.

ACKNOWLEDGEMENT

The authors would like to thank their colleagues Messrs. G.G. Piepers, J. Marchés, C. van der Harst, N. van Bezooyen, B.W. Treijtel, C. van der Laan, H.J.J. van Ballegoy and H.E. Huynink for their aid in carrying out the experiments and their inventivity in solving many of the practical problems.

REFERENCES

[1] G.H.J. Broers; "High temperature galvanic fuel cells"; thesis University of Amsterdam (1958).

[2] G.H.J. Broers; Dechema Monographien Bd. 38, 277 (1960), Verlag Chemie G.m.b.H., Weinheim, W. Deutschland.

[3] "Fuel Cells", Vol. 1, Chapt. 6. G.J. Young (Ed.), Reinhold, New York, (1960).

[4] "Fuel Cells", Vol. 2, Chapt. 2. G.J. Young (Ed.), Reinhold, New York, (1963).

[5] G.H.J. Broers; in "Fuel Cells, a C.E.P. Technical Manual", p. 90, Am. Inst. of Chem. Engineers, New York (1963).

[6] G.H.J. Broers, M. Schenke and G.G. Piepers; J.Advanced Energy Conversion 4, 131 (1964).

[7] E. Justi and A. Winsel; "Kalte Verbrennung - Fuel Cells", Chapt. 9.3. Steiner, Wiesbaden (1962).

[8] "Fuel Cells"; W. Mitchell Jr. (Ed.); Chapt. 5 and Chapt. 9; Acad. Press. New York and London (1963).

[9] R.W. Hardy and J. McCallum; in Reference [5], p. 45.

[10] K. Bischof and E. Justi; Jahrb. Akad. Wiss. Lit. (Mainz), 250 (1955).

[11] I. Trachtenberg; J. Electrochem. Soc. 111, 110 (1964).

[12] G.H.J. Broers and M. Schenke; J. Advanced Energy Conversion; to be published.

[13] E.J. Cairns, A.D. Tevebaugh and G.J. Holm; J. Electrochem. Soc. 110, 1025 (1963).

E.J. Cairns and A.D. Tevebaugh; J. of Chem. and Eng. Data 9, 453 (1964).

[14] G.H.J. Broers and B.W. Treijtel; submitted to J. Advanced Energy Conversion.

[15] H.H. Chambers and A.D.S. Tantram; in Reference [3], Chapt. 7, p. 105

[16] R. de Levie, Thesis, University of Amsterdam (1963); Electrochim. Acta 8, 751 (1963).

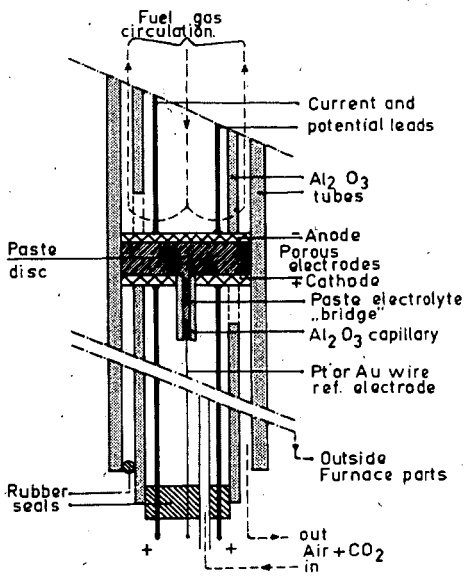

Fig.1 Disc cell with reference electrode for polarization and other fundamental studies.

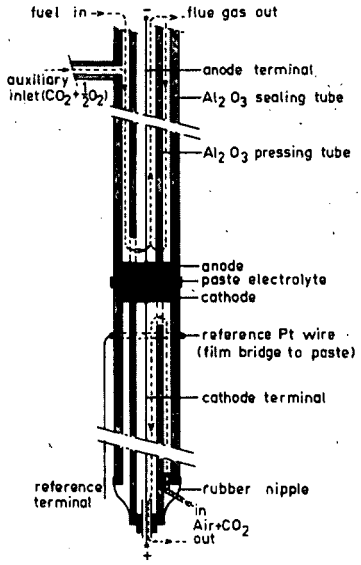

Fig.2 Simplified version of the cell cf. Fig.1.

Electrolytic bridge from reference wire to paste disc formed spontaneously by creeping of the molten salt.

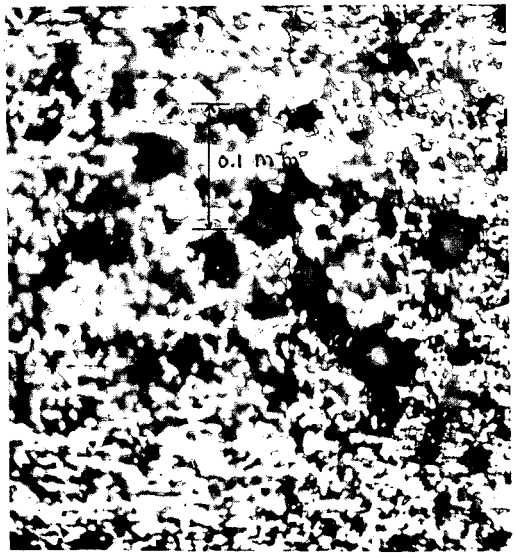

Fig.3a Porous Ni electrode (Mond Nickel Co.) before use. Magnification 125x, before final reproduction.

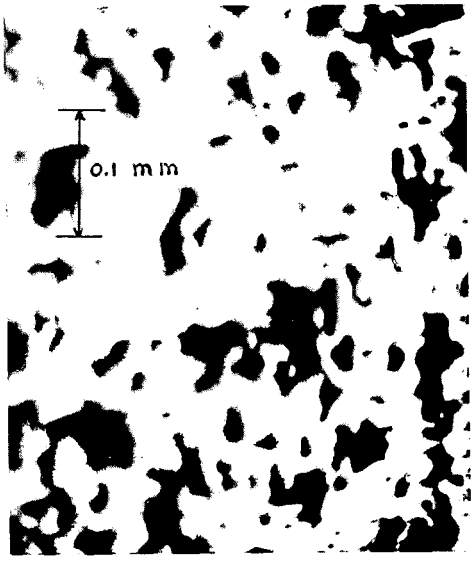

Fig.3b The same material after 625 hours of continuous anodic operation at 100 mA/cm², 700 °C.

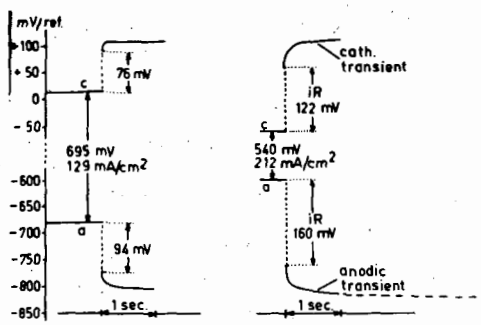

Fig.4a.
Determination of iR drop and electrode polarization by means of fast current interruption (< 2 μsec).

Linear time scale.

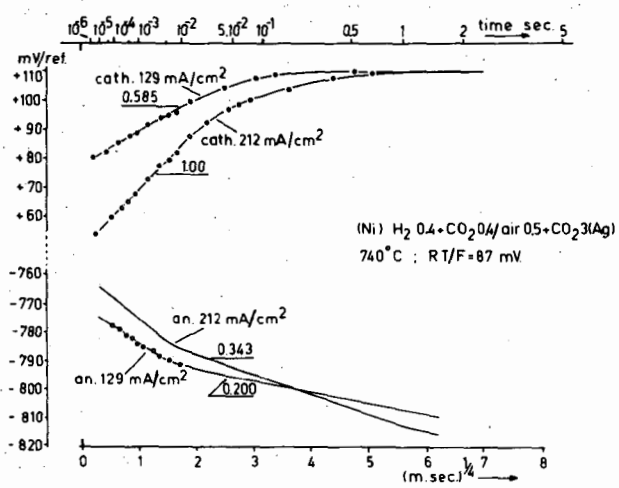

Fig.4b.

Cathodic and anodic potential transients cf. Fig.4a, but plotted on a $t^{\frac{1}{4}}$ time scale.

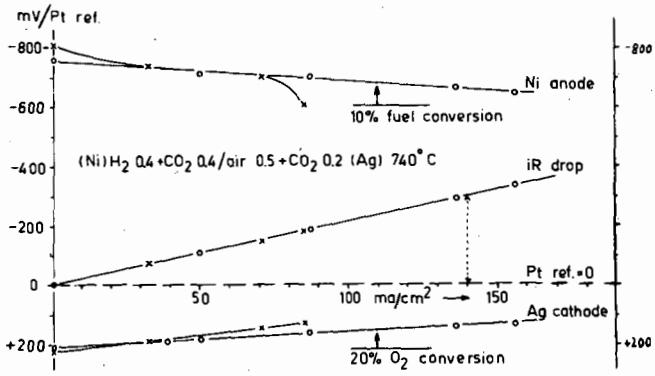

Fig.5. Steady state (iR free) potentials and iR drop of a cell cf. Fig.2, as functions of the current density. Cathode : Ag - powder, anode :"fiber nickel". x-x-x : 3rd day of operation; o-o-o-o :18th day of operation.

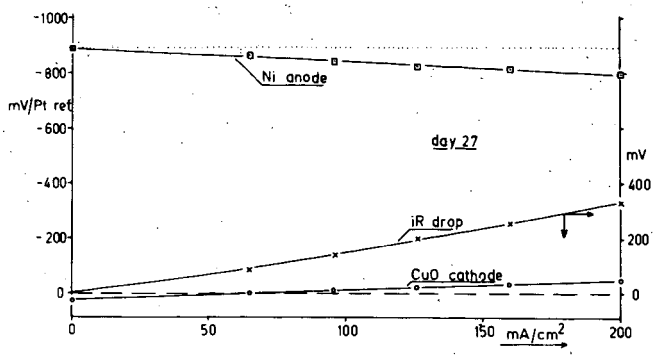

Fig.6a. Steady state potentials and iR drop of a cell with CuO cathode and Ni anode, 27th day of operation.

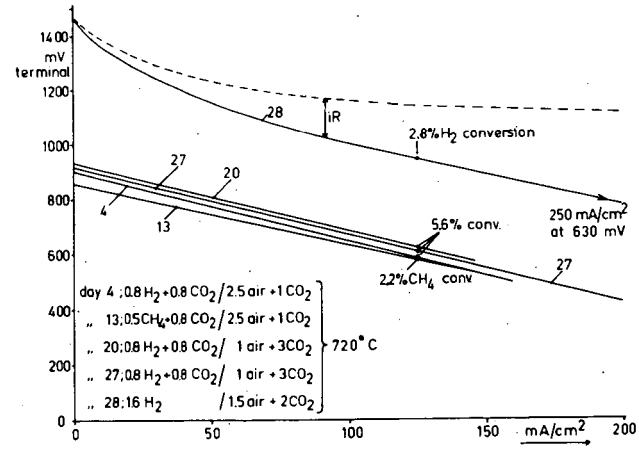

Fig.6b. Terminal voltage vs.current density characteristics of the cell cf. Fig.6a, over a 4 week period. No iR drop corrections, except upper curve (dashed).

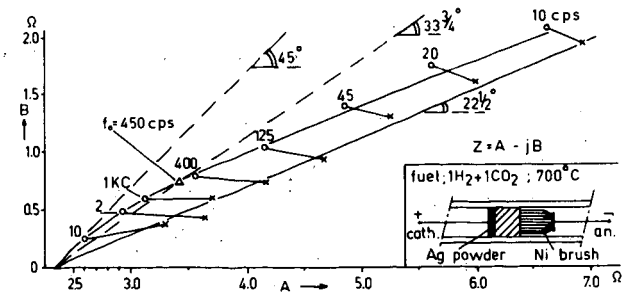

Fig.7. A.C.impedance vector diagram (Argand diagram) of a nickel brush electrode, simulating an ideally homoporous system. o-o-o : points observed; x-x-x : impedances corrected for influence of double layer capacity. Drawn straight line : theoretical prediction for pure diffusion control; 22½° slope, $|Z| \cdot f^{1/2}$ = constant.

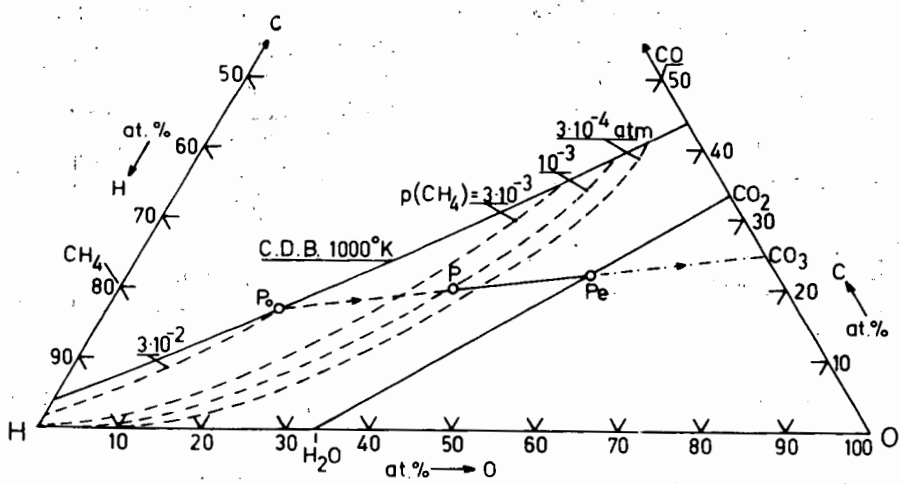

Fig.8. C-H-O triangular diagram, representing at 1000°K and 1 atm : 1) Carbon deposition boundary (CDB) ; 2) Equilibrium partial pressure "isobars" of CH_4 (dashed); 3) Oxidation path PP_e of the standard fuel P , reacting with $CO_3^{=}$ ions ; 4) Optimal fuel composition P_o that may be oxidised along the same path.

P corresponds with 32% oxidation of P_o .

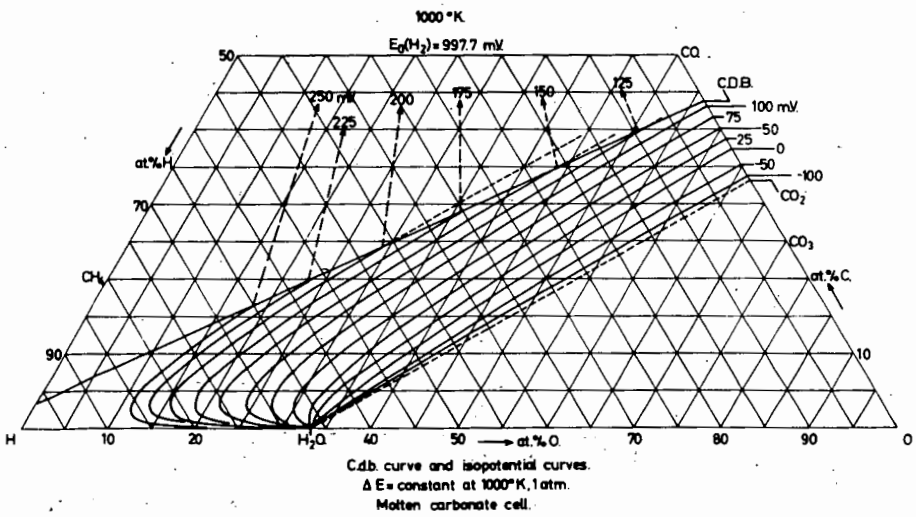

Fig.9. C-H-O diagram with CDB and curves of constant EMF with regard to fuel composition, for molten carbonate cells at 1000°K , 1 atm.

$E(cell) = E_o(H_2) + \Delta E(anodic) + \Delta E(cath.)$; cf. Eq.(2).

$\Delta E(anodic)$ can be read directly from the diagram, in mV.

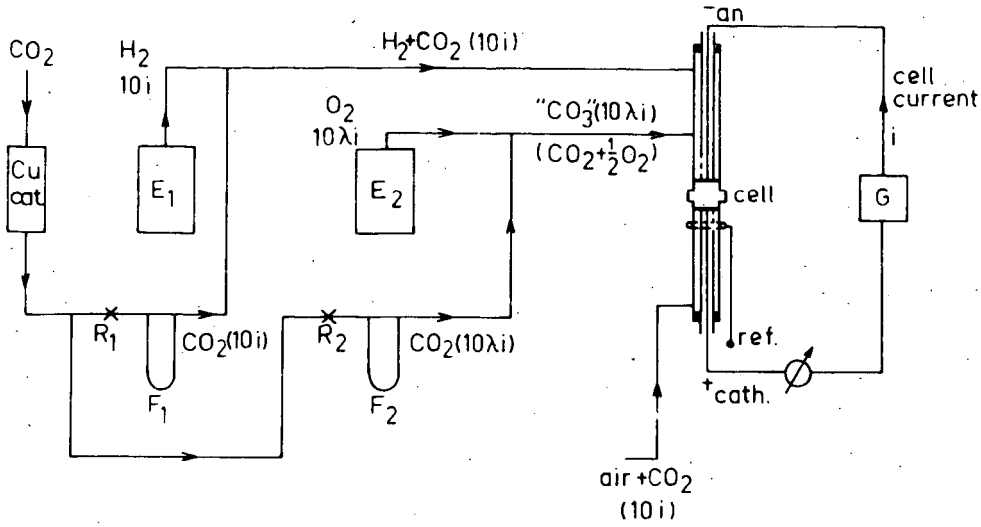

Fig.10. Determination of fuel utilization in an imaginary 10 cell series battery, by means of a single cell. E_1 : H_2 electrolyzer; E_2: O_2 electrolyzer; F_1 and F_2: CO_2 flowmeters with regulating valves R_1 and R_2 ; G : galvanostat. Cell cf. Fig.2.

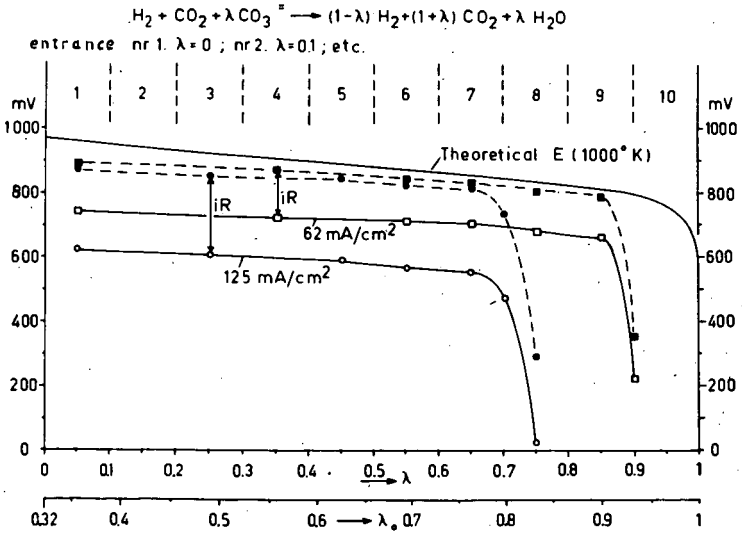

Fig.11. Results of fuel utilization experiments at 62 mA/cm² and 125 mA/cm². λ is the conversion degree relative to point P in Fig.8, λ_0 similarly to point P_0 in Fig.8. Anode: "fiber nickel", cathode: Ag screen. T=720°C. Theoretical E based upon equilibrium composition of the fuel mixture; derived from Fig.9 and Eqs.(1c)& (2).

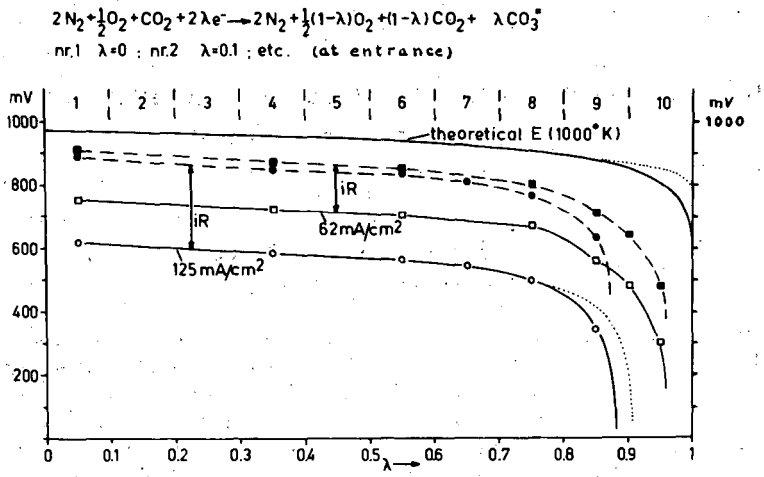

Fig.12. Results of oxidant utilization experiments. Points indicated: equal conversion degrees of O_2 and CO_2. Dot curve: $\lambda(O_2)$ held at 0.8 , $\lambda(CO_2) \geqslant 0.8$. (Similarly for the theoretical E curve.)

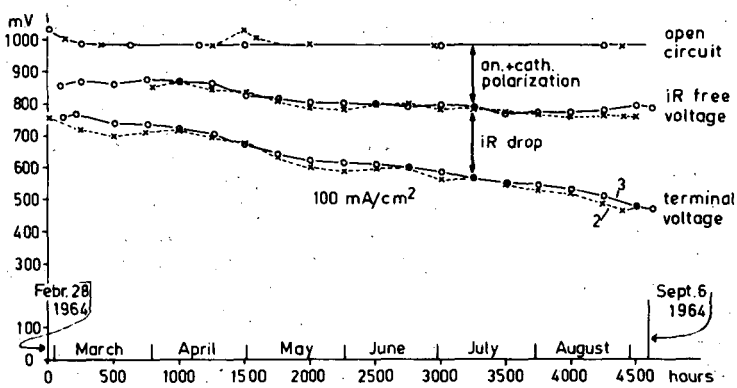

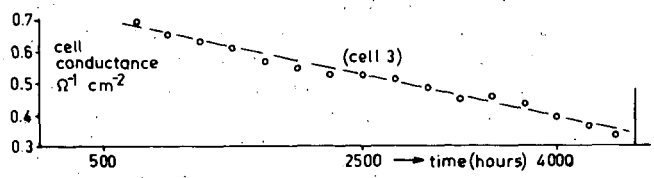

Fig.13. Long run (~6 months) output voltages of twin cells 2 (x-x-x) and 3 (o-o-o) at 700°C and 100 mA/cm², continuously. Fuel: 1 H_2 + 1 CO_2 , 10% conversion; oxidant: 2.5 air + 1 CO_2 , 10% conversion. Anode: "Clevite nickel"; cathode: Ag screen.
Lower section: decrease of cell conductance in the same period.